

# Doxorubicin (DOX) Gadolinium–Gold-Complex: A New Way to Tune Hybrid Nanorods as Theranostic Agent

This article was published in the following Dove Press journal:  
*International Journal of Nanomedicine*

Memona Khan<sup>1</sup>  
Sarah Boumati<sup>2</sup>  
Celia Arib<sup>1</sup>  
Amadou Thierno Diallo<sup>1</sup>  
Nadia Djaker<sup>1</sup>  
Bich-thuy Doan<sup>2</sup>  
Jolanda Spadavecchia<sup>1</sup>

<sup>1</sup>CNRS, UMR 7244, CSPBAT, Laboratoire de Chimie, Structures et Propriétés de Biomatiériaux et d'Agents

Thérapeutiques, Université Sorbonne Paris Nord, Bobigny, 93000, France; <sup>2</sup>CNRS UMR 8060, iCLeHS, Synthèse, Electrochimie, Imagerie et Systèmes Analytiques Pour le Diagnostic SEISAD, Chimie ParisTech, Université PSL, Paris, 75231, France

Correspondence: Bich-thuy Doan  
CNRS, UMR 8060, iCLeHS, Synthèse, Electrochimie, Imagerie et Systèmes Analytiques Pour le Diagnostic SEISAD, Chimie ParisTech, PSL University, 11 Rue Pierre et Marie Curie, Paris Cedex 05, Paris, 75231, France  
Email bich-thuy.doan@chimieparitech.psl.eu

Jolanda Spadavecchia  
CNRS, UMR 7244, CSPBAT, Laboratoire de Chimie, Structures et Propriétés de Biomatiériaux et d'Agents Thérapeutiques, Sorbonne Paris Nord University, 1 rue chablis, Bobigny, 93000, France  
Email jolanda.spadavecchia@gmail.com

**Introduction:** In this paper, we have designed and formulated, a novel synthesis of doxorubicin (DOX) loaded bimetallic gold nanorods in which gold salt (HAuCl<sub>4</sub>) is chelated with anthracycline (DOX), diacid polyethylene-glycol (PEG-COOH) and gadolinium salt (GdCl<sub>3</sub> \* 6 H<sub>2</sub>O) to form DOX IN-Gd-AuNRs compared with DOX ON-Gd-AuNRs in which the drug was grafted onto the bimetallic pegylated nanoparticle surface by electrostatic adsorption.

**Material and Method:** The physical and chemical evaluation was performed by spectroscopic analytical techniques (Raman spectroscopy, UV-Visible and transmission electron microscopy (TEM)). Magnetic features at 7T were also measured. Photothermal abilities were assessed. Cytotoxicity studies on MIA PaCa-2, human pancreatic carcinoma and TIB-75 hepatocytes cell lines were carried out to evaluate their biocompatibility and showed a 320 fold higher efficiency for DOX after encapsulation.

**Results:** Exhaustive physicochemical characterization studies were conducted showing a mid size of 20 to 40 nm diameters obtained with low polydispersity, efficient synthesis using seed mediated synthesis with chelation reaction with high scale-up, long duration stability, specific doxorubicin release with acidic pH, strong photothermal abilities at 808 nm in the NIR transparency window, strong magnetic r<sub>1</sub> relaxivities for positive MRI, well adapted for image guided therapy and therapeutical purpose in biological tissues.

**Conclusion:** In this paper, we have developed a novel theranostic nanoparticle composed of gadolinium complexes to gold ions, with a PEG biopolymer matrix conjugated with anti-tumoral doxorubicin, providing multifunctional therapeutic features. Particularly, these nano conjugates enhanced the cytotoxicity toward tumoral MIAPaCa-2 cells by a factor of 320 compared to doxorubicin alone. Moreover, MRI T<sub>1</sub> features at 7T enables interesting positive contrast for bioimaging and their adapted size for potential passive targeting to tumors by Enhanced Permeability Retention. Given these encouraging antitumoral and imaging properties, this bimetallic theranostic nanomaterial system represents a veritable promise as a therapeutic entity in the field of medicinal applications.

**Keywords:** hybrid nanorods, doxorubicin, MRI, MIAPaCa-2 cells, hyperthermia

## Introduction

Lately, hybrid gold nanomaterials have been broadly applied as drug delivery vehicles to cancer cells due to their optochemical,<sup>1,2</sup> thermoplasmonics<sup>3,4</sup> and chemical ability of functionalization.<sup>5-9</sup> Various types of hybrid nanomaterials and inorganic nanoparticles as Gold (Au) NPs,<sup>10</sup> silver,<sup>11</sup> and iron oxide NPs,<sup>12</sup> have already shown a therapeutic activity against cancer. Among all, gold nanorods

(AuNRs), are achieving high emphasis for many reasons as follows: (i) Au NPs do not show any toxicity and reactivity and thus are suitable for *in vivo* studies; (ii) they display remarkable optical properties as the generation of localized surface plasmons (LSPR);<sup>13</sup> (iii) their nature enables the easy surface chemical functionalization<sup>14</sup> and (iv) their size, morphology, and monodispersity can be monitored during the synthesis process, allowing their optical properties from the visible to the near-infrared region (NIR) region.<sup>15</sup> Compared with other gold nanoparticles (AuNPs), Au nanorods (AuNRs) are particularly interesting due to their anisotropic structure. Indeed, AuNRs exhibit better NIR absorption compared with other gold nanostructures<sup>16,17</sup> with efficient photothermal heat conversion for photo-treatment.<sup>18</sup> Previously, Xiao et al<sup>19</sup> have proved that AuNRs conjugated with doxorubicin (DOX) can be applied as efficient multifunctional nano-platform for both targeting and imaging cancer cells. Doxorubicin (DOX), an anticancer anthracycline drug, shows strong side effects, including myelosuppression and cardiotoxicity.<sup>20</sup> In order to enhance the chemotherapeutic drug efficiency, the drug can be loaded on the surface of nanostructures,<sup>21,22</sup> such as to improve the bioavailability, sustained drug release and biocompatibility.<sup>23</sup>

In the last years, Spadavecchia et al have designed and synthesized a novel nano-therapeutic vector based on a gold-doxorubicin complex called DOX INPEG-AuNPs.<sup>24</sup> This protocol was implemented to encapsulate any drugs with a capacity for complexation to gold salts, such as carboxylates, phosphonates, including anthracycline, alkaloid and flavonoid molecules.<sup>25,26</sup> This chemical methodology (Method IN) has been compared with other grafting methodologies in which the drug was functionalized onto gold surface by carbodiimide chemistry (EDC/NHS)<sup>27</sup> or electrostatic adsorption EA (Method ON).<sup>28,29</sup>

On the basis of Method IN, the same authors have conceived new chemical polymeric bimetallic nanostructures, in which gadolinium ions complex to gold ions, and then stack with a biopolymer matrix to form a hybrid nanoparticle.<sup>30</sup> Gadolinium is a chemical element widely used as a contrast agent to improve the quality of MRI images for more efficient diagnosis in cancer or inflammation.

MRI is a non-invasive, non-radiative technique, which is widely used clinically but often requires the injection of contrast agents to improve specificity for diagnosis leading to enhanced contrast and sensitivity.<sup>31</sup> The intensity of the

signal is based on the density of water protons and is modulated by their longitudinal ( $T_1$ ) and transverse ( $T_2$ ) relaxation times.

$Gd^{3+}$  complexes are most commonly used to enhance the relaxation rate of water protons and thus increase image contrast.<sup>32</sup> The efficiency of a contrast agent is characterized by its relaxivity that depends mainly on the rotational correlation time ( $\tau_R$ ) of the complex, the number of coordinated water molecules ( $q$ ) and the lifetime of these water molecules in the inner coordination sphere ( $\tau_m$ ). Three main strategies have been developed to improve the efficiency of Gd based contrast agents (CA): (i) combine CA to macromolecules (such as nanoparticles, polymers, proteins or liposomes) to increase the  $Gd^{3+}$  payload and to enhance in the same time the  $\tau_R$ ; (ii) use ligands that enable more than one water molecules to be coordinated to the  $Gd^{3+}$ ; (iii) increase the exchange rate of the inner sphere water molecules. By using self-assembly, large structures can be easily obtained and should present slower rotational dynamics, thus enhanced relaxivity.<sup>33</sup>  $Gd^{3+}$  complexed with polymers ligands, is the most used contrast agent in clinics. However free  $Gd^{3+}$  is a toxic element because it has the same ionic radius as  $Ca^{2+}$ , which is an important element for biological processes. This similarity can lead to the competition between the two of them. Lanthanide ions such as  $Gd^{3+}$  can bind to the  $Ca^{2+}$  enzymes or replace the  $Ca^{2+}$  ions in cell membrane channels, and lead to the inhibition of biological processes<sup>34</sup> inducing deleterious toxic effects. Therefore, some measures have to be taken to reduce this toxicity by adding ligands such as DOTA.<sup>35</sup> The Gd ions would become biocompatible when it is chelated with a biopolymer.

Complexation of  $Gd^{3+}$  to Gold nanoparticles has already been reported in recent works.<sup>30</sup>

Intense research are conducted in the development of novel theranostic MRI contrast agent in middle size to nanoparticulate size with triggering for drug release or intelligent contrast activation.<sup>36</sup>

In the current study, four aims were carried out: first, we designed and synthesized bimetallic Gadolinium–Gold Nanorods (Gd-AuNRs) by a fast modification of “seed mediated synthesis” implying hybrid Gd-AuNRs with a mixture of capping polymers (diacid PEG and CTAB). Second, we combined our bimetallic nanorods with doxorubicin (DOX) through chelation process (DOX IN-Gd-AuNRs) and electrostatic functionalization (DOXON-Gd-AuNRs) in order to investigate their

efficacy after internalization in pancreatic MIA PaCa-2 and hepatocytes TIB-75 cells with a consecutive test to confirm an excellent property as imaging contrast agent (third aim). We also suggested a photothermal study of these nanostructures in order to develop a multitask nanovector with a highly effective cancer therapy feature (fourth aim). These highlights headline the potential of the chemical approach to study DOX-gadolinium-gold interactions in relation to drug delivery and drug targeting activity.

## Experimental Section

### Materials

The reagents, tetrachloroauric acid ( $\text{HAuCl}_4 \cdot 3\text{H}_2\text{O}$ ), gadolinium chloride hexahydrate ( $\text{GdCl}_3 \cdot 6\text{H}_2\text{O}$ ), sodium borohydride ( $\text{NaBH}_4$ ), dicarboxylic polyethylene glycol (PEG)-600 diacid, L-Ascorbic acid (AA), hexadecyltrimethylammonium bromide ( $\geq 99,9\%$ -Sigma, CTAB), silver nitrate ( $\text{AgNO}_3$ ) and doxorubicin hydrochloride (DOX) were purchased from Sigma-Aldrich (Saint-Quentin Fallavier, France). All these chemicals were used as received without further purification. Ultrapure MilliQ water was used throughout the experiments.

### Physical-Chemical Characterization

All measurements were performed in triplicate in order to confirm the reproducibility of the synthetic and analytical procedures.<sup>24,25</sup>

### UV-Vis Absorption Spectroscopy

Absorption spectra were recorded using a double-beam Varian Cary 500 UV-Vis spectrophotometer (Agilent, Les Ulis, France). Absorption spectra of the Gd-AuNRs were recorded in the 350–900 nm spectral range in water.

### Transmission Electron Microscopy (TEM)

Transmission electron microscopy (TEM) images were recorded with a JOEL JEM 1011 microscope (JOEL, Tokyo, Japan) operating at an acceleration voltage of 100 kV. TEM specimens were prepared after separating the surfactant from the particles by centrifugation. Typically, 1 mL of Gd-AuNRs was centrifuged for 20 min at a speed of 12,000 rpm. The upper part of the solution was removed and the solid portion was redispersed in 1 mL of water. A total of 2  $\mu\text{L}$  of this redispersed particle suspension was placed on a carbon-coated copper grid manufactured by Smethurst High-Light Ltd (Elektron

Technology, Cambridge, UK) and marketed exclusively by Agar Scientific (Essex, UK) and dried at room temperature. The Raman experiments were conducted on an Xploraspectrophotometer (Horiba Scientific), which was equipped with a Helium-Neon (HeNe) laser of 785 nm. A CCD camera was used for data acquisition. Optical filter was set at 100% so that the laser power used is 8 mW. The density of diffraction grating was used at 600 features/mm which offers a spectral resolution of  $12\text{cm}^{-1}$ . The confocal hole (pinhole) resulted at 300  $\mu\text{m}$ .

### Scanning Electron Microscopy-Energy Dispersive X-Ray Analysis (SEM-EDX)

Scanning electron microscopy (SEM) investigation was performed on an environmental SEM microscope (ESEM, Quanta 200 FEG, FEI Company Hillsboro, OR) equipped with an EDX spectrometer (Genesis 2000, XMS System 60 with a Sapphire Si/Li Detector from EDAX Inc., Mahwah, NJ).

### Magnetic Resonance Imaging (MRI)

In vitro relaxivity experiments were carried out by recording  $T_1$  and  $T_2$  maps with a 7T MR micro imaging vertical spectrometer fitted with an ultra-shielded refrigerated magnet (300WB, Bruker, Avance II, Wissembourg, France) equipped with a nominative 200 mT/m actively shielded gradient and a 40 mm Bruker linear birdcage coil, at 273 K with the method described previously.<sup>30</sup>

The  $T_1$  and  $T_2$  relaxation times of a set of 4 solutions of Gd-Au nanoparticles prepared at different concentrations (0, 0.1, 0.2, 0.5, 1 mM of  $\text{Gd}^{3+}$  in saline) were measured.

Molar relaxivities  $r_1$ , and  $r_2$  in  $\text{mM}^{-1} \cdot \text{s}^{-1}$  were obtained using the following:

$$\frac{1}{T_y} = r_y[\text{Gd}] + \frac{1}{T_{y,0}} \text{ with } y: 1 \text{ or } 2$$

The relaxivity  $r_1$  was determined by fitting the slope of the relaxation rate ( $R_i$ ,  $\text{s}^{-1}$ ) as a function of the  $\text{Gd}^{3+}$  concentration in mM using Excel software.

Values of relaxivities  $r_1$  and  $r_2$  are expressed in ( $\text{mM}^{-1} \cdot \text{s}^{-1}$ ) and corrected from ICP AES elementary analysis (Institut Physique du Globe (IPG) ICP AES Facility, and ENSCP Paris);  $r_2/r_1$  ratio is calculated to evidence the  $T_1$  type MRI contrast agent ( $>1$ ).

### Hyperthermia/Phototherapy

Aqueous solutions of AuNRs (1 mL) were introduced in a quartz cuvette and irradiated with an 808 nm continuous

laser (Focuslight, China) at laser irradiance ( $0.5 \text{ W/cm}^2$ ) for 15 min at room temperature (296 K). The temperature was recorded every 15 s with a digital thermometer using a thermocouple probe (Hanna Instruments, USA).

## Synthesis Procedures of AuNRs

Gold Nanorods (AuNRs) were synthesized by a modification of seed-mediated procedures.

First step was to prepare the seed solution by mixing 5 mL of aqueous  $\text{HAuCl}_4$  solution (0.5 mM) with 5 mL of CTAB solution (0.1 M) for 3 min. Then, 1.2 mL of ice-cold 8 mM  $\text{NaBH}_4$  was added dropwise, which resulted in the formation of a brown color solution.

The solution was stirred for more than 3 min and kept at 298 K without agitation for 4hrs.

The growth solution was prepared by mixing 5 mL of an aqueous solution of  $\text{HAuCl}_4$  (1 mM) with 2.5 mL of CTAB (0.1 M) for 3 min. Then, 250  $\mu\text{L}$  of diacid polyethylene glycol 600 (PEG) (1 mM) and 250  $\mu\text{L}$  of  $\text{AgNO}_3$  (7.06 mM) were added to the stirring solution  $\text{HAuCl}_4$ -CTAB. After 3 min of additional stirring, 630  $\mu\text{L}$  of ascorbic acid (15 mM) was added dropwise to the solution. The color of the growth solution changes from dark yellow to colorless. The final step was the dropwise addition of 40  $\mu\text{L}$  of the seed solution to the growth solution. The final solution was kept covered for 30 min without agitation. The color of the solution changes over the period depending on the final size of the nanorods. The resulting pink/violet solution was centrifuged and purified.

## Synthesis Procedures of Gd-AuNRs

Seed solution was prepared by mixing 5 mL of aqueous  $\text{HAuCl}_4$  solution (0.5 mM) with 5 mL of  $\text{Gd}^{3+}$  solution (40 mM) under magnetic stirring during 3 min. After this time, 5 mL of CTAB (0.1 M) was added to the stirring solution until formation of homogeneous solution. Then, 1.2 mL of ice-cold 8 mM  $\text{NaBH}_4$  was added dropwise, until complete reduction and consequently formation of brown color solution. The solution was stirred for more than 3 min and kept at 298 K without agitation for 4hrs.

The growth solution was prepared by mixing 5 mL of an aqueous solution of  $\text{HAuCl}_4$  (1 mM) with 5 mL of  $\text{Gd}^{3+}$  (40 mM) for 3 min under stirring at room temperature. After this time, 2.5 mL of an aqueous solution of surfactant CTAB (0.1 M). Then, 250  $\mu\text{L}$  of diacid polyethylene glycol 600 (PEG) and 250  $\mu\text{L}$  of  $\text{AgNO}_3$  (7.06 mM) were added to the stirring solution  $\text{HAuCl}_4$ -  $\text{Gd}^{3+}$ -CTAB-PEG. After 3 min of more stirring 630  $\mu\text{L}$  of ascorbic acid (15 mM)

was added dropwise to the solution. The color of the growth solution changes from dark yellow to colorless. Forty microliters of seed solution was added to a growth solution. The final solution was kept covered in the dark for 30 min without agitation. The color of the solution changes over the period depending on the final size of the nanorods. The resulting pink/violet solution was centrifuged and purified. Stock solutions were stored at 27–29 °C and characterized using UV–vis, Raman spectroscopy and Transmission Electron Microscopy (TEM).

## Conjugation of DOX Onto Gd-AuNRs (DOX ON-Gd-AuNRs)

One milliliter of the DOX solution (1.7 mM) was added to the Gd-AuNRs solution (13.7 mL;  $[\text{Au}]$ : 0.363 mM). This mixture was kept for 1 h under agitation at room temperature. Next, the resulting DOX ON-Gd-AuNRs solution was centrifuged twice at 6000\*g for 10 min to remove excess of DOX, and the pellets were redispersed in 0.5 mL of water milli Q.

## Synthesis Procedures of DOX Inside Gd-AuNRs (DOX IN-Gd-AuNRs)

Seed solution was prepared by mixing 5 mL of aqueous  $\text{HAuCl}_4$  solution (0.5 mM) with 1 mL of DOX (1.7 mM) solution for 3 min. Then, 5 mL of  $\text{Gd}^{3+}$  solution (40 mM) was added to the stirring solution. Afterwards, 5 mL of CTAB (0.1 M) was added under stirring for 3 min. Then, 1.2 mL of ice-cold 8mM  $\text{NaBH}_4$  dropwise, which resulted in the formation of a dark pink color solution. The solution was stirred for 3 min more and kept at 298 K without agitation for 4hrs.

The growth solution was prepared by mixing 5 mL of an aqueous solution of  $\text{HAuCl}_4$  (1 mM) with 1 mL of DOX (1.7 mM) solution for 3 min. Afterwards 5 mL of  $\text{Gd}^{3+}$  (40 mM) was added under stirring for 3 min. After this time, 2.5 mL of an aqueous solution of surfactant CTAB (0.1 M) was added under stirring. Then, 250  $\mu\text{L}$  of diacid polyethylene glycol 600 (PEG) (1 mM) and 250  $\mu\text{L}$  of  $\text{AgNO}_3$  (7.06 mM) were added to the stirring solution  $\text{HAuCl}_4$ -  $\text{Gd}^{3+}$ -CTAB-PEG. After 3 min, 630  $\mu\text{L}$  of ascorbic acid (15 mM) was added dropwise to the solution. The color of the growth solution changes from dark yellow to colorless. The final step was the dropwise addition of 40  $\mu\text{L}$  of the seed solution to the growth solution. The final solution was kept covered for 30 min without agitation. The resulting brown solution was centrifuged and purified at the same conditions and

characterized by UV-Vis spectroscopy, Transmission Electron Microscopy (TEM), and Raman spectroscopy.

### Quantification of Free Gd<sup>3+</sup>

The amount of free gadolinium is determined by using xylenol orange method<sup>37</sup> with UV-Vis spectrometer. The solution was prepared in acetic buffer solution (pH= 5.8). The ratio of absorbance at 573 nm and 433 nm is proportional to the free Gd<sup>3+</sup> concentration. Calibration curve was obtained by spectrophotometric changes of xylenol orange absorption in the presence of different amounts of Gd<sup>3+</sup> (Figure S1 in Supporting Information). The amount of free gadolinium was determined by using the equation of calibration curve:  $y = 19991x + 0.0744$  where  $x$  is the concentration of free gadolinium.

### Determination of Hybrid Gold Nanorods (Gd-AuNRs, DOX IN-Gd-AuNRs, DOX ON-Gd-AuNRs) Concentration

Gd-AuNRs concentration was determined by exploiting standard mathematical calculations in colloidal solution. Lambert–Beer law ( $A = \epsilon cl$ ) was used to determine colloids concentration. In this equation  $A$  is the maximum absorbance (corresponding to the Surface Plasmon Resonance Band at around 540–800 nm) of the UV-visible spectrum,  $\epsilon$  is the molar extinction coefficient (equal to  $3.07 * 10^{10} \text{ M}^{-1} \text{ cm}^{-1}$ ),  $C$  is the molar concentration of colloids and  $l$  is the optical length of cuvette (1 cm). The resulting  $C$  was multiplied for the dilution factor to obtain the concentration of colloids.

### Stability of Hybrid Gold Nanorods (Gd-AuNRs, DOX IN-Gd-AuNRs, DOX ON-Gd-AuNRs)

The stability of Hybrid Gold Nanorods was detected by UV-Vis profiles. One milliliter of each colloidal solution at  $2.4 * 10^{-4} \text{ M}$  (Gd-AuNRs, DOX IN-Gd-AuNRs, DOX ON-Gd-AuNRs) were dissolved in DMEM during 72 h (Figure S2 in Supporting information).

### Cell Culture

Both cell lines, MIA PaCa-2, a human pancreatic carcinoma cells and TIB-75 murine hepatocytes cells were purchased from American Type culture collection (ATCC). The two cell lines were grown in DMEM (Gibco, Bio-Sciences Ltd, Ireland) supplemented with

10% FBS (Sigma-Aldrich) in a humidified atmosphere at 37°C and 5% CO<sub>2</sub>.

### Cytotoxicity Tests

For the cytotoxicity tests, cells were plated into 96-wells at 4000 cells per well in 100  $\mu\text{L}$  of culture medium. They were maintained in a 5% CO<sub>2</sub>-humidified. After 24 h, the medium was removed and replaced by new medium containing nanoparticles without and with 9 different concentrations of DOX: 1  $\mu\text{M}$ , 0.5  $\mu\text{M}$ , 0.25  $\mu\text{M}$ , 0.125  $\mu\text{M}$ , 0.0625  $\mu\text{M}$ , 0.03125  $\mu\text{M}$ , 0.0156  $\mu\text{M}$ , 0.0078  $\mu\text{M}$ , 0.0039  $\mu\text{M}$  and 0  $\mu\text{M}$ . The cytotoxicity was evaluated with two tests, resazurin/Alamar blue and MTT. All analyses for IC50 calculations were computed using GraphPad Prism software.

### DOX Loading Efficiency

The amount of the drugs (DOX) incorporated into Gd-AuNRs was measured by UV-Vis absorption spectroscopy and extrapolate the DOX concentrations by a calibration curve<sup>24</sup> (Figure S3 in Supporting Information).

### Drug Release from Gd-AuNRs

DOX releases were evaluated at physiological temperature (37° C). Drug-loaded AuNRs were dispersed at concentration of  $1.3 * 10^{12}$  particles/mL in 1.0 mL PBS and submitted to dialysis as previously described<sup>21</sup>. The concentration of drug released from AuNPs was expressed as a percentage of the total drug concentration present in the sample as in the following equation and plotted as a function of time.

$$\% \text{ DOX released} = \frac{\text{Concentration of drug released}}{\text{Initial drug concentration}} \times 100$$

## Results and Discussion

Our aim was to design bimetallic hybrid gold nanorods (Gd-AuNRs), tuning the chemical physical characteristics based onto better steric arrangement of the doxorubicin (DOX) onto gold surface of nanoparticles combining chelation process (Method IN) and Electrostatic Adsorption (EA) (Method ON).

### Formation Mechanism of Gd-AuNRs

Several authors have studied the association between Au nanoparticles and Gd chelates through the synthesis of Gd-chelate-gold nanorods,<sup>38</sup> Gd-enriched DNA AuNPs conjugates,<sup>39</sup> and grafting Gd chelates on gold nanostructures or hydroxyapatite<sup>40</sup> as multimodal MRI/CT

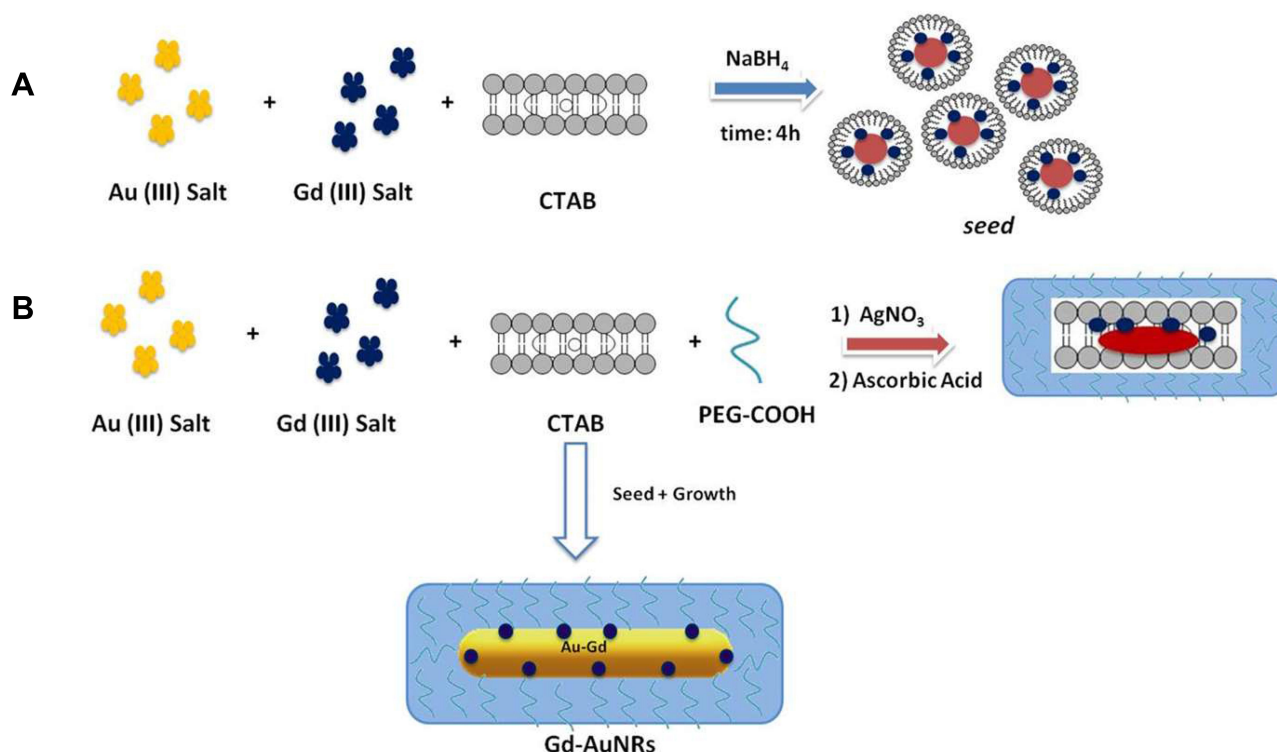
contrast agents. Previously Spadavecchia et al have investigated the mechanism of bimetallic hybrid nano formulations as spherical and polyedrical shape, including Au-Gd complex wrapped into a biocompatible polymer structure.<sup>30</sup> The same authors have studied the competition effect with several capping agents on the growth process of hybrid nanoparticles.<sup>41</sup> Based on these findings, we conceived a novel chemical protocol to obtain bimetallic nanorods (Gd-AuNRs) through modification of seed mediated procedures by complexation method. The first step (Scheme 1 panel A) displays the seed formation by interaction of tetrachloroauric acid in the presence of gadolinium salt to form gold-gadolinium clusters  $Gd^{3+}-Au^{3+}$  in ultrapure water solution at room temperature. The addition of CTAB as surfactant allows a disproportionate reaction in aqueous phase. Indeed, as reported earlier, the extraordinarily strong binding of Gd-AuBr<sub>2</sub> to the positive CTAB<sup>+</sup> head group could stabilize the Au<sup>+</sup> species in aqueous solution. This is due to the cooperative effect of micelles and Br<sub>2</sub>, which favours the emergence of soluble Au<sup>+</sup> ions. Finally, the complete reduction by strong reducing agent (NaBH<sub>4</sub>) gives the formation of gadolinium-gold seed particles. The second step (Scheme 1 panel B) provides the formation of

growth solution by interaction of bimetallic micelles (Gd-Au-CTAB) with diacid PEG. We believe that PEG and CTAB compete during the synthetic process owing to a higher collision rate of CTAB-Au-Gd micelles than that of PEG-Au-Gd. This effect is responsible for the change in the final NPs shape due to a probable deposition of PEG molecules onto Au facet [110].

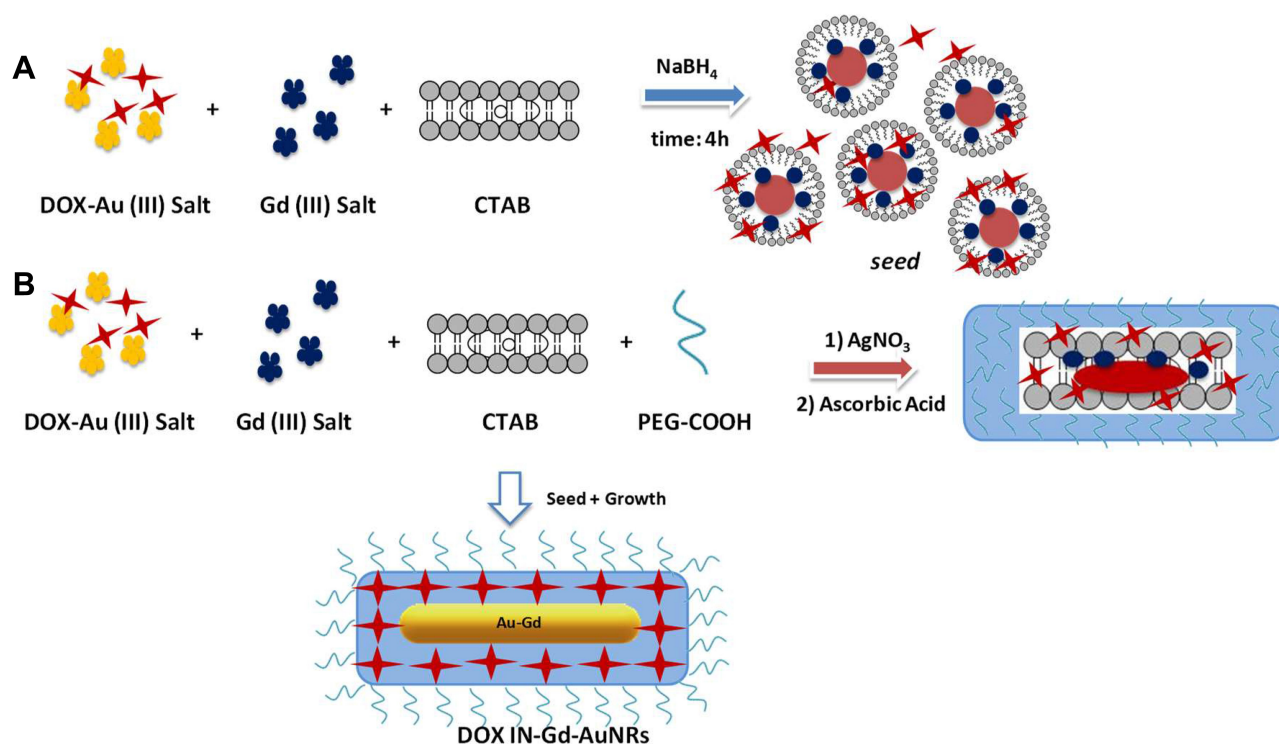
## Doxorubicin (DOX) Complexation into Gd-AuNRs (DOX IN-Gd-AuNRs)

Previously Spadavecchia et al have conceived an original methodology called “Method IN” in which DOX and other several drugs or biomolecules were chelated with gold salt and polymers to form hybrid gold nanoparticles with high biological therapeutic effect.<sup>24,28,29,42</sup>

On the basis of this methodology, we adapted the similar protocol to “seed mediated synthesis” in order to obtain DOX IN Gd-AuNRs. The first and second steps have in common both seed and growth solution consisted of Au (III)-DOX complexation, (DOX-AuCl<sub>2</sub><sup>-</sup>) and generation of gold clusters<sup>24</sup> (Scheme 2 panel A) that react with gadolinium salt and CTAB in order to form hybrid metallomicelles.



**Scheme 1** Schematic representation of seed mediated synthesis of bimetallic nanorods (Gd-AuNRs).



**Scheme 2** Cchematic representation of seed mediated synthesis of DOX-IN-Gd-AuNRs.

The second step of seed formation provides a strong reduction in order to obtain doxorubicin-Gd-Au-seeds. In this present study, CTAB was in the seed solution as micelle, at the concentration of 0.92 mM. In this experimental condition, the amino groups of DOX are partially deprotonated ( $pK_a = 5.4$ , pH of the seed solution is 6) and may heavily interact with positively charged end-groups of the CTAB micelles. The presumable DOX-Gd-AuCl<sub>2</sub>-CTAB complexes subsequently interact leading to a reduction of gold salts.

In addition, electrostatic intermolecular interactions may improve the side-by-side arrangement of the CTAB-DOX complexes, due to electronic structure of DOX rich in delocalized electrons which enhances its involvement in the reduction of the gold salt, before the addition of NaBH<sub>4</sub>. In the case of growth solution, we assume the formation of a presumable CTAB-DOX-Au-Gd complexes, the same reduction process involving ascorbic acid may occur. The further reduction of Au I can then proceed via an electron transfer at the surface of electron-rich, CTAB-DOX-Au-Gd capped, seed particles (Scheme 2 panel B). This steric arrangement of DOX during synthetic process of bimetallic nanorods (Gd-AuNRs) was evaluated by UV-Vis absorption spectroscopy, TEM and

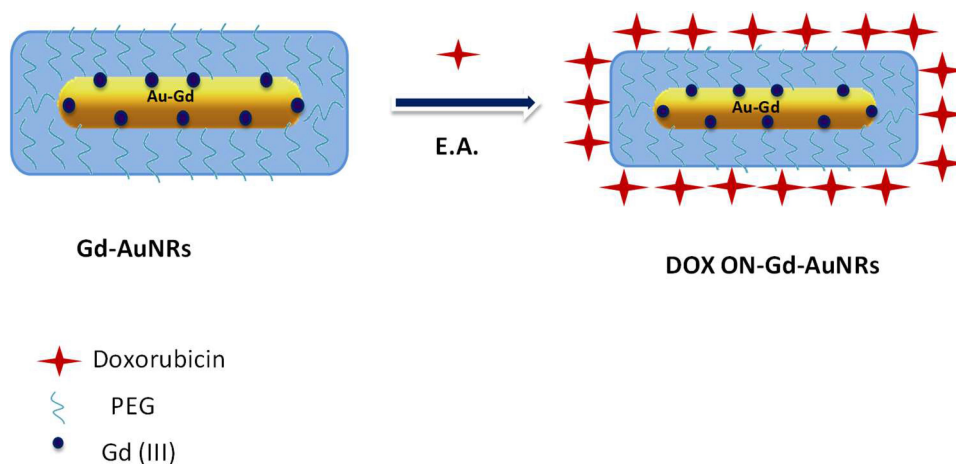
Raman Spectroscopy and will be reported in the following section.

## Doxorubicin (DOX) Conjugation Onto Gd-AuNRs (DOX ON-Gd-AuNRs)

Previously other authors have functionalized DOX molecules onto AuNRs, Gd<sub>2</sub>O<sub>3</sub> nanoparticles and bimetallic AuNRs by several methodologies as encapsulation, electrostatic adsorption and/or covalent approach. In order to compare the influence of steric arrangement of the drug onto nanoparticle surface, DOX was conjugated on the surface of pegylated Gd-AuNRs via Electrostatic Adsorption (EA) between the charged amino residues ( $-NH_3^+$ ) onto the skeletal of DOX with the polar surface of pegylated chains onto Gd-Au surface (Scheme 3).

## Spectroscopic Analysis and Characterization

The seed-mediated growth is the most popular method for the synthesis of colloidal AuNRs due to the simplicity of the procedure, high quality and yield of nanorods, ease of controlling particle size, and flexibility for further chemical modifications.<sup>43</sup>



**Scheme 3** Schematic representation of Electrostatic Adsorption of DOX onto Gd-AuNRs.

Figure 1A, black line displays the localized surface plasmon resonance (LSPR) bands of Gd-AuNRs with a strong resonance band at around 868 nm corresponding to the longitudinal plasmon oscillation<sup>44</sup> and a weaker

one at ca 525 nm corresponding to the transverse plasmon oscillation band confirming the presence of elongated Gd-AuNRs isolated from each other (Figure 1B, panel 1).

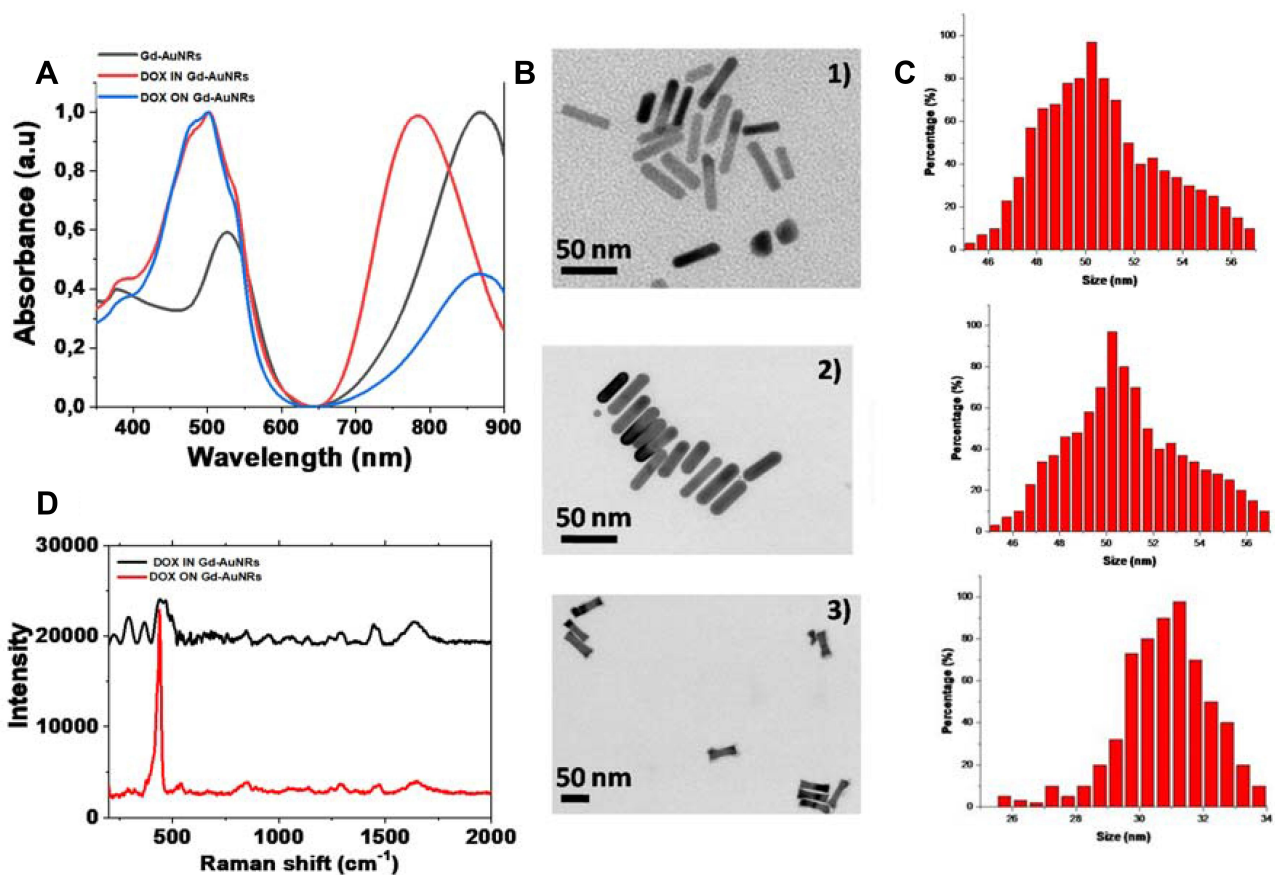


**Figure 1** (A) Normalized UV-Vis absorption of GdAuNRs (blackline), DOX IN-Gd-AuNRs (red line) and DOX ON-Gd-AuNRs (blue line); (B) TEM images of Gd-AuNRs (panel 1), DOX IN-Gd-AuNRs (panel 2) and; DOX ON-Gd-AuNRs (panel 3) and (C) their corresponding histogram size distribution; (D) Raman spectra of DOX IN-Gd-AuNRs products (black line) and DOX ON-Gd-AuNRs (red line). Experimental conditions:  $\lambda_{exc} = 785$  nm; laser power 20 mW; accumulation time 180 s.

Following the modification of classical shape-directing CTAB-controlled seeding growth procedure, we indeed obtained a solution of gadolinium gold nanorods (Gd-AuNRs), well dispersed in shape and size; the anisotropic growth of nanoparticles into nanorods is known to be due to the preferential binding of CTAB+ ligands to the [100] faces of the seed nanoparticles; this has been attributed to the gold atom spacing on this rather open face, closer to the size of the surfactant head groups than that on the close-packed rod end surfaces. In our case, the presence of diacidPEG in growth solution generates a competition between CTAB+ and PEG-COO<sup>-</sup> with consequently different adsorption onto gold [100] faces. Note that the absence of nanorod aggregation in solution is obviously due to the electrostatic repulsions between positively charged ligands. After grafting of DOX to the Gd-AuNRs by electrostatic adsorption (DOX ON-Gd-AuNRs), we observe the appearance of peaks at 485 nm, 503 nm, and 537 nm characteristics of DOX and a strong decrease in the longitudinal surface plasmon resonance peak (Figure 1A, blue line), with a tendency of the nanorods to self assemble in linear chains (Figure 1B, panel 2).

In addition, the color of the solution changed from violet to pink pale upon attachment of DOX to the nanorods.

When DOX molecules participate in the nucleation and growth process of bimetallic nanorods, we observe a consequent change of plasmonic properties. UV-Vis absorption spectroscopy analysis of DOX IN-Gd-AuNRs (Figure 1A, red line) showed a characteristic absorption bands<sup>11</sup> due to the presence of DOX. This behavior was associated to  $\pi$ - $\pi^*$  electronic transitions due to interactions between the DOX ring and Gd-AuCl<sub>2</sub><sup>-</sup> ions and gives a clear evidence of the complex formation. This band is due to electronic delocalization of aromatic ring and HOMO-LUMO transition and explains the increase in intensity at 540 nm. This confirms that DOX was effectively involved into the nucleation process and creates a complex with Au-Gd. We also observe a strong blue shift of longitudinal Plasmon peak from 868 nm to 783 nm (Figure 1A, red line) related to DOX unwrapping<sup>45</sup> on nanorod surface. Indeed this behavior might come from the optical properties of DOX itself.<sup>46</sup> TEM images showed a characteristic rod shape for Gd-AuNRs (Figure 1B, panel 1) with a diameter of about 50 nm (see histogram Figure 1C, panel 1); after complexation of DOX into Gd-AuNRs (DOX IN-Gd-AuNRs), we can see a tendency of the nanorods to self assemble as side by side chains<sup>47</sup> with a decrease of the size to 40 nm (see histogram Figure 1C panel 2), compared to DOX ON-Gd-AuNRs, in which we observe a size of

nanorods with about 31 nm (see histogram Figure 1C, panel 3).

Zeta potential measurements show that, Gd-AuNRs, DOX ON-Gd-AuNRs and DOX IN-Gd-AuNRs were colloidally stable at physiological pH. This stability was enhanced with the presence of the PEG coating.<sup>27</sup> However, DOX IN-Gd-AuNRs display a better stability in DMEM (10% FBS) during 72 h compared to Gd-AuNRs and DOX ON Gd-AuNRs in which we observe a decrease of plasmon peaks after 24 h.

We also characterized our bimetallic hybrid nanorods by Raman spectroscopy (Figure 1D). As previously described, Raman spectrum of DOX in water showed a very intensive peak at 463 cm<sup>-1</sup>, followed by several small bands between 600 and 1000 cm<sup>-1</sup> as well as several intense bands from 1200 to 1700 cm<sup>-1</sup>. In our case, Raman spectrum of the case of DOX IN-Gd-AuNRs (Figure 1D, black line) showed a very intense peak at 343 cm<sup>-1</sup> and a doublet at 226–286 cm<sup>-1</sup>. These bands are due to the gold chloride stretches and  $\delta$  (O-Au-O) in ring F<sup>24</sup> confirming the presence of DOX-AuCl<sub>2</sub> in solution. The spectrum also shows several small bands between 400 and 500 cm<sup>-1</sup> that are assigned to  $\delta$  in Phe A, B, C and F rings close to the broad bands observed experimentally. Such peak assignments were based on the fact that the O-O electronic transition are expected.<sup>35</sup> Many weak peaks were observed in the region 400–1200 cm<sup>-1</sup>, as well as an intense doublet at 1259–1430 cm<sup>-1</sup>, surrounded by medium peaks at 1232, 1279 and 1332 cm<sup>-1</sup>. Furthermore, DOX ON-Gd-AuNRs (Figure 1D, red line) showed a strong peak at 430 cm<sup>-1</sup> due to the vibrations  $\delta$ (OH ... O),  $\nu$ (OH ... O) of the PEG that confirm a different steric arrangement of PEG molecules compared to DOX IN-Gd-AuNRs. The peak at 1730 cm<sup>-1</sup> was assigned to the C=O of the ester bond linking PEG-diacid molecules to gold surface of nanorods. A small peak at 1640 cm<sup>-1</sup> was also present, representing the characteristic band of DOX molecules. All spectra also exhibit peaks at 324, 660 and 1630 cm<sup>-1</sup> due to vibrations of Gd-OH and Gd-Cl in bimetallic nanorods,<sup>48</sup> confirmed by EDX measurements with comparative spectra as previously described.<sup>30</sup>

## Stability, Loading and Drug Release of DOX IN-Gd-AuNRs, DOX ON-Gd-AuNRs

The stability of DOX IN-Gd-AuNRs and DOX ON-Gd-AuNRs in solution, plays a key role to assess therapeutic

applications, and was analysed by monitoring the Raman longitudinal band of the Gd-AuNRs ([Figure S2 panel A in Supporting Information](#)). Analysis was performed in DMEM under 72 h. A decrease of longitudinal band confirms an aggregation of bimetallic nanorods. The synthesized DOX IN-Gd-AuNRs showed an almost negligible change in the longitudinal band position over a period of 72 h ([Figure S2 panel B in the Supporting Information](#)). Although the band intensity slightly decreased overtime, we could conclude that no major agglomeration occurred over 72 h, implying that DOX IN-Gd-AuNRs might find application as clinical drug-delivery systems. Zeta potential measurements confirmed the spectroscopic results, showing that DOX IN-Gd-AuNRs were colloidal stable at physiological pH (zeta-potential =  $-30 \pm 1$  mV with a PDI equal to 0.331). Contrarily to DOX IN-Gd-AuNRs, DOX ON-Gd-AuNRs showed an agglomeration after incubation in DMEM ([Figure S2 panel C in Supporting Information](#)). We suggest that DOX IN-Gd-AuNRs enhanced stability is due to the presence of the PEG polymer chains on the nanoparticle surface.

Kumar et al<sup>49</sup> have monitored the loading and release of DOX onto Gd<sub>2</sub>O<sub>3</sub> nanoparticles by microemulsion method with a sustained release of the drug at pH 7.4 and 5 of about 65% after 165 h for pH 7.4 and 90% after 167 h for pH 5.0. Other authors,<sup>45</sup> have synthesized, multifunctional gold nanorods coated with alternating layers of the anionically charged poly(styrene sulfonate) (PSS) and the cationically charged poly(lysine) (PLL) polymers to mask the toxic hexadecyltrimethyl ammonium bromide (CTAB) layer. In this formulation DOX was released after 96 h reached ca. 40 and 20% in contrast to 85 and 50% at physiological pH in presence of trypsin. In our previous work, we have monitored the loading and release of DOX onto pegylated spherical gold nanoparticles named AuNPsin which DOX was grafted onto the gold surface by carbodiimide chemistry (Method ON) or complexed with gold salt (Method IN), in which the DOX loading efficiency was 86.5% and the release was pH- and time-dependent for DOX IN-Gd-AuNRs with release at acidic pH (~98%), after 96 h, nine-fold higher than at neutral pH (~10%). Contrarily, in the case of DOX ON-Gd-AuNRs doxorubicin release into an aqueous environment measured in previous works, was almost negligible after 7 days, at both pH suggesting that drug release from Gd-AuNRs was triggered by enzymatic activity DOX release into aqueous environment was almost negligible (2%) at both pH.<sup>50</sup>

In the present novel formulations of Gd-AuNRs, DOX assumes a different chemical and sterical conformation compared to recent synthesis approach in which the drug molecules reside inside the AuNR core. The successful loading ratios of DOX onto Gd-AuNRs, in both configuration (IN and ON) were evidenced by the characteristic absorption peaks at 485 nm from DOX ([Figure S3 in Supporting information](#)). The standard absorption of DOX was plotted in the inset of figure ([Figure S3 in Supporting information](#)) according to UV-Vis absorbance spectra of DOX at various concentrations. In the case of DOX IN-Gd-AuNRs, the loading efficiencies were estimated to be 93% with 9.0  $\mu\text{g}$  present in  $2.3 \times 10^{-8}$  mol of NPs. DOX releases were pH- and time-dependent ([Figure 2A and B](#)). A sustained drug release was observed in the first 5 h for both drugs at pH 4 and 7, which is highly favorable for drug delivery as the cancer cells thrive in acidic conditions. We presumed that the release of DOX was checked by an ionic equilibrium between Au (III)-PEG complexes trapped into Gd-AuNRs by the electrostatic interactions between PEG chains, CTAB and ionic drug. As previously described, the mechanism by which acidic pH triggers drug release is probably associated to the presence of carboxylate groups in the chemical structure of PEG molecules. In the case of DOX ON-Gd-AuNRs ([Figure 2B](#)) the loading efficiencies were estimated to be 83% and the releases were pH- and time-dependent at acidic pH (~75%), after 96 h, compared to neutral pH (~30%).

## Cytotoxicity

The cytotoxicity of these nanorods was evaluated on two types of cell lines, TIB-75 (hepatocytes) and MIA PaCa-2 (pancreatic cells) by using resazurinAlamar blue and MTT cytotoxic tests for better robustness with increasing concentration of DOX in nanoparticles from 0 to 1  $\mu\text{M}$ , and simultaneously increasing concentrations of Gd and Au ([Figure 3](#)).

Both MIA PaCa-2 and TIB-75 cells were exposed to a series of DOX IN-Gd-AuNRs and DOX ON-Gd-AuNRs dilutions in complete media (DMEM+10% FBS) (concentrations ranging from 0 to 1  $\mu\text{M}$  of DOX in Gd-AuNRs). To evaluate the potential toxicity coming from the AuNRs themselves as controlled AuNRsnanovectors, we also tested the cytotoxicity of AuNRs (without Gd or DOX), and Gd-AuNRs without DOX (concentrations ranging from 0 to 2.9  $\mu\text{M}$  of Au).

The percentage (%) of living cells (MIA PaCa-2 and TIB-75) was evaluated with spectroscopy UV-Vis (MTT) or

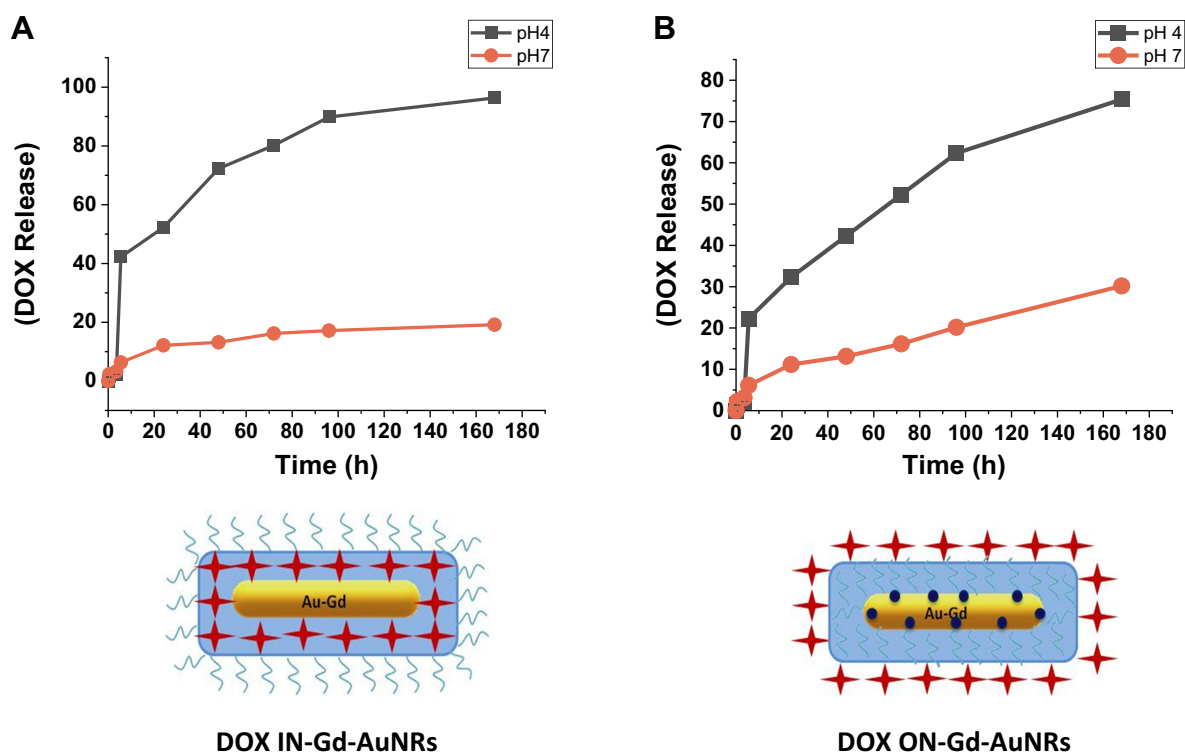


**Figure 2 (A)** Percentage (%) of DOX released from DOX IN-Gd-AuNRs and **(B)** DOX ON-Gd-AuNRs overtime in PBS (37°C). Data are reported as average  $\pm$  standard deviation (n= 3).

fluorescence (resazurin) after exposure of 24h with AuNRs, Gd-AuNRs, DOX IN-Gd-AuNRs, DOX ON-Gd-AuNRs, DOX alone (Figure 3) and results are summed up in Table 1.

IC<sub>50</sub> of AuNRs without DOX or Gd<sup>3+</sup>, and IC<sub>50</sub> of Gd<sup>3+</sup> and DOX alone were measured in addition to those of the final theranostic DOX-Gd-AuNRs in order to distinguish the cytotoxicity of them.

Figure 3A displays the cytotoxicity of DOX alone with IC<sub>50</sub> of 15.6  $\mu$ M and 25.6  $\mu$ M for respectively MIA PaCa-2 and TIB75 cells line. Figure 3B shows the cytotoxicity results of AuNRs. The IC<sub>50</sub> for MIA PaCa-2 is 5.05  $\mu$ M and 4.7  $\mu$ M (in Au concentration) for TIB-75. The AuNRs are therefore mildly toxic for both cells lines.

Figure S4 in Supporting Information shows the cytotoxicity result of Gd-AuNRs.

As we can see in the table, the IC<sub>50</sub> for MIA PaCa-2 is 2.15 $\mu$ M and 2.05 $\mu$ M (Au) for TIB-75.

The cytotoxicity of Gd-AuNRs is 2 times higher than AuNRs.

As we can see in the Table 1, IC<sub>50</sub> of the AuNRs is higher than IC<sub>50</sub> of Gd-AuNRs by a factor of 2.35 (2.15 $\mu$ M/5.05  $\mu$ M in Au) which means Gd-AuNRs are therefore more toxic than AuNRs. This increase of toxicity can be explained by the amount of free Gd<sup>3+</sup>

released from the AuNRs after cells interaction or internalization compared with AuNRs (without Gd). However, the dosage of free Gd<sup>3+</sup> by spectroscopic quantitative studies have shown a small (6%) of free Gd<sup>3+</sup> in solution, providing a low toxicity coming from free Gd<sup>3+</sup>. The IC<sub>50</sub> of Gd<sup>3+</sup> for both cells lines are also very high (2947  $\mu$ M and 2547  $\mu$ M), showing that these small amount of Gd<sup>3+</sup> remaining in solution is not the leading cause of cytotoxicity.

Figure 3C shows the cytotoxicity result of DOX IN-Gd-AuNRs. The IC<sub>50</sub> for the MIA PaCa-2 is 0.045 $\mu$ M and 0.158 $\mu$ M (DOX) for TIB-75. The cytotoxicity of DOXIN-Gd-AuNRs is also about twice to three times higher on pancreatic MIA PaCa-2 cell lines than on reference hepatocytes TIB-75 cell lines, in coherence with the tumoral features of MIA PaCa-2 cells.

In literature, IC<sub>50</sub> of DOX is 14.25  $\mu$ M for MIA PaCa-2 cell line, here it is 320–390 times smaller when conjugated into the AuNRs.<sup>51</sup> This result could be rationalized by the internalization of AuNRs inside the cells and that the high encapsulation into nanoparticles of DOX, increases its efficiency as antitumoral molecule by a factor of around 300, confirming the strong interest of the novel Gd-Au theranostic nanoparticles.

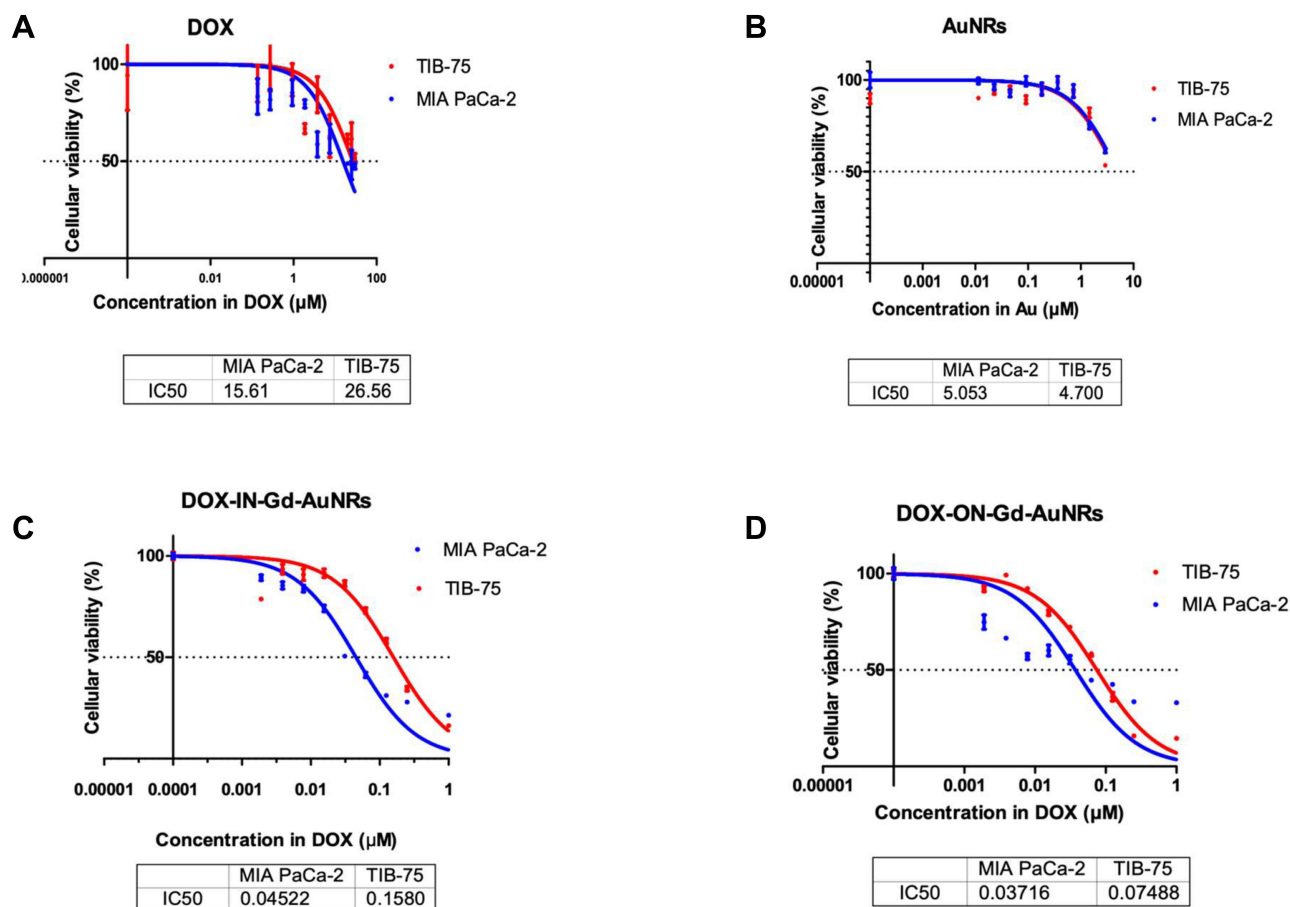


**Figure 3** Cytotoxicity MTT tests with two cell lines (MIA PaCa-2, TIB-75); IC50 values are expressed at different concentrations of Au, Gd and DOX. (A) DOX alone; (B) AuNRs; (C) DOX IN -Gd-AuNRs; (D) DOX ON-Gd-AuNRs.

Figure 3D shows the cytotoxicity result of DOX ON-Gd-AuNRs. The IC50 for MIA PaCa-2 is 0.037μM and for TIB-75 0.075μM (DOX). IC50 of DOX ON-Gd-AuNRs is similar to DOX IN-Gd-AuNRs. The efficiency of DOX ON-Gd-AuNRscan be due to facile release of the drug inside the cells as the drug is on the surface of Gd-AuNRs.<sup>30</sup>

To sum up, the cytotoxicity results of DOXIN-Gd-AuNRs and DOXON-Gd-AuNRs were translated by calculating IC50 of each compound such as Gd<sup>3+</sup>, Au<sup>3+</sup> and DOX of the AuNRs. The results show that the cytotoxicity comes mainly from DOX encapsulated in AuNRs. Plus as shown in the Table 1, the main interesting result from the cytotoxicity study is that the IC50 of Gd-AuNRs

**Table 1** IC50 in Two Cell Lines as Function of Au, DOX and Gd<sup>3+</sup> Concentration (μm)

IC50 (μM) in MIA PaCa-2 and TIB-75 Cell Lines/AuNRs Formulations	AuNRs	Gd-AuNRs	DOX-IN-Gd-AuNRs	DOX-ON-Gd-AuNRs	Gd <sup>3+</sup>	DOX
[Au]	5.05 4.70	2.15 2.05	0.32 0.89	0.16 0.45		
[Gd]		96.61 96.00	12.76 31.38	6.90 15.68	2907 2547	
[DOX]			0.05 0.15	0.04 0.07		15.61 26.56

in DOX concentration is about 300 times more efficient than DOX alone, demonstrating the high potentiality provided by the Gd-AuNRs to vectorize the antitumoral molecule into the cells.

## Release and Biological Mechanism of Internalization

As shown in the previous paragraph, only 6% of gadolinium is free in colloidal solution. The IC<sub>50</sub> of Gd<sup>3+</sup> free is approximately 3000  $\mu$ M or 3 mM. So we can conclude that the cytotoxicity comes from discharge of DOX inside the cells which can be translated as the internalization of nanoparticles and cells (Figure 3).

## MRI

The  $r_1$ relaxivity of the AuNRs has been measured and surprisingly, the values at 7T were twice greater than commercial DOTA Gd (Dotarem). As the dosage of free Gd<sup>3+</sup> shows a low release of about 6% from the Gd-AuNRs and a stability of the structure of the AuNRs on keeping the complexed Gd<sup>3+</sup> ions, this very promising value encouraged us to further pursue relaxivity and MRI experiments as a potential MRI contrast agent and theranostic scaffold. MRI Images of T<sub>1</sub> weighted sequence (Figure 4) display bright signal from Gd concentrated solutions in saline (arrow).

The T<sub>1</sub> weighted and T<sub>2</sub> weighted images recorded at 7T of the various samples at increasing Gd<sup>3+</sup> concentration

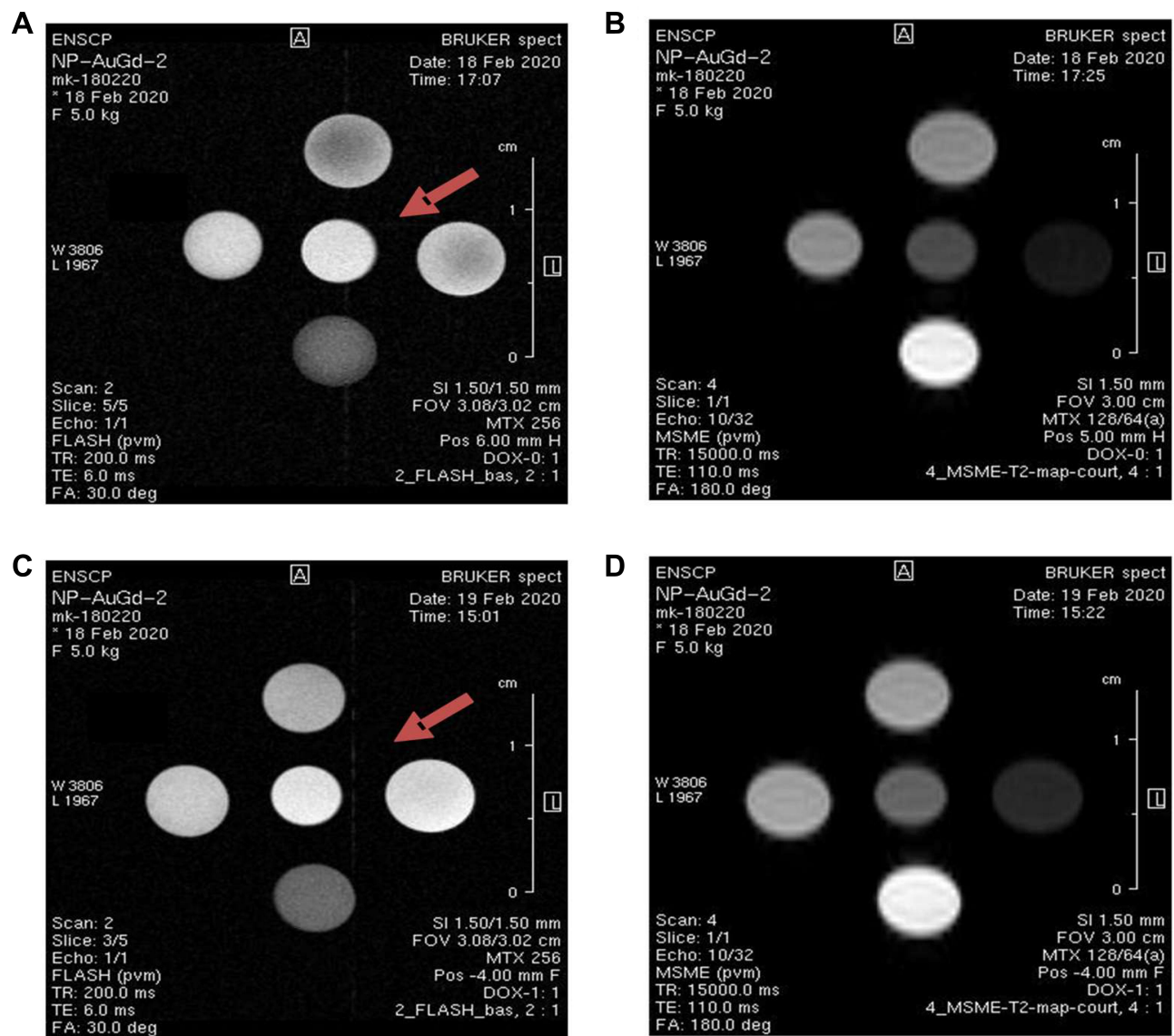


**Figure 4** Examples of T<sub>1</sub> and T<sub>2</sub> weighted M<sub>R</sub> images of Gd-AuNRs: alone (**A** and **B**), respectively, DOX IN-Gd-AuNRs (**C** and **D**).

**Table 2** Table of  $R_1$  and  $R_2$  Relaxivities Values Measured at 7T, 273 K, Corrected with the ICP AES Elementary Analysis

Contrast Agents	$r_1$	$r_2$	$r_2/r_1$
DOTAREM	4.0	3.9	1.1
Gd <sup>3+</sup>	9.5	5	1.9
DOX-IN-Gd-AuNRs	9.7	14.5	1.5
DOX-ON-Gd-AuNRs	8.8	10.8	1.2

display clear hypersignal and hyposignal respectively, as expected for  $T_1$  and  $T_2$  contrast agents.

The measured relaxivities for all Gd-Au nanoparticles without and with DOX are unexpectedly high at 7T (Table 2). We believe that these increased relaxivities are due to the combined water access to the inner sphere of the Gd<sup>3+</sup> ions within the nanoparticle, which drives principally the  $r_1$  relaxivity. The Gd<sup>3+</sup> water environment inside the polymeric should be similar to the one from the hydrated sphere of Gd<sup>3+</sup> free in solution.

In 14 mM of Gd-AuNRs, 0.6–0.7mM of free gadolinium (6%) contents were determined after 24h.<sup>52</sup>

The analysis of free Gd<sup>3+</sup> shows that a minor 6% amount of free Gd<sup>3+</sup> are released in solution and that the high relaxivities value are due to Gd<sup>3+</sup> incorporated within the polymeric structure of the AuNRs, where water molecules are also solubilized.

Moreover, the nanoparticles of Gd<sup>3+</sup> complexes degrees of freedom related to the rigidity of the nanostructure would reduce their tumbling rate leading to increased  $r_1$  relaxivity.

The high  $r_2$  values evidence the encapsulation of Gd<sup>3+</sup> into the AuNRs in coherence with magnetic susceptibility effects of nanoparticles. There have been reports of nephrogenic systemic fibrosis (NSF) associated with the use of linear chelator-based CA in the past decade. For this reason, there are increasing demands for macrocyclic efficient chelator-based CAs and such strategy will be applied to design a novel higher biocompatible theranostic nanoparticle.

## Plasmonic Characterization

It is well known that the LSPR wavelength is determined by the AuNRs parameters like the shape, the size, the surrounding medium of the AuNRs and their chemical composition. Gold and silver are the most studied plasmonic materials which have a maximum of the LSPR wavelength in the visible and near infrared spectral region. However, one has to note that, among them, gold

nanoparticles (AuNPs) are considered as the most viable biomedical materials due to their physical and chemical properties.<sup>53,54</sup> In addition, several works show that some biomolecules are used to modify the surface properties of gold nanostructures.<sup>29,55</sup> This important approach is a very attractive strategy, as it leads to a new generation of hybrid nanomaterials. It is also important to use large nanoparticles in order to maximize the ratio between scattering and absorption cross sections of metallic nanoparticles. This is due to the fact that under quasi-static approximation, it can be obtained that the ratio between scattering and absorption of a spherical particle is proportional to  $d^3$ , where  $d$  is the particle diameter.<sup>56,57</sup> On the other hand, increasing the size of the nanoparticle leads to a red shift of the LSPR wavelength. In this case, gold nanorods (AuNRs) are very suitable agents for thermal destruction of cancer cells due to their photothermal heating ability.<sup>58–60</sup> Figure 5 shows the extinction spectra of AuNRs in different dielectric environments (water, DOX and Gd<sup>3+</sup>).

As shown in the results, the extinction spectra of the four nanorods solutions have one high peak resonance corresponding to the LSPR mode in the near-IR part (longitudinal resonance of the plasmons across the long axis of the NR, 700–1000 nm) and a secondary damped peak in the green part of the spectrum (transversal resonance along the short axis of the NR at 526 nm). For DOX IN-Gd-AuNRs and DOX ON-Gd-AuNRs, the transversal mode is affected by the DOX absorption around 480 nm. Previous works demonstrated that the LSPR peak for noble metal nanoparticles is extremely sensitive to the external dielectric environment,<sup>61,62</sup> especially the longitudinal mode in the case of AuNRs. As shown in Figure 5, AuNRs show a longitudinal LSPR peak at 725 nm, Gd-AuNRs and DOX ON-Gd-AuNRs at 868 nm, while for DOX IN-Gd-AuNRs, the LSPR peak is around 780 nm. The LSPR peak is shifted to higher wavelength when the refractive index of the medium increases as expected.<sup>63</sup>

## Photothermal Heating

Figure 6 shows the temperature elevation characteristic in the different solutions with and without AuNRs versus time, with concentrations of DOX (1.7 mM), Gd (40 mM), AuNRs (Au: 0.577 mM), Gd-AuNRs (0.363 mM in Au), DOX IN-Gd-AuNRs, (0.341 mM in Au), DOX ON-Gd-AuNRs (0.341 mM in Au). The different solutions were exposed to 0.5 W/cm<sup>2</sup> excitation laser density during 15 minutes at 808 nm wavelength to evaluate their temperature elevation in the perspective of photothermal therapy application. During laser heating of AuNRs suspended in buffer solution, the

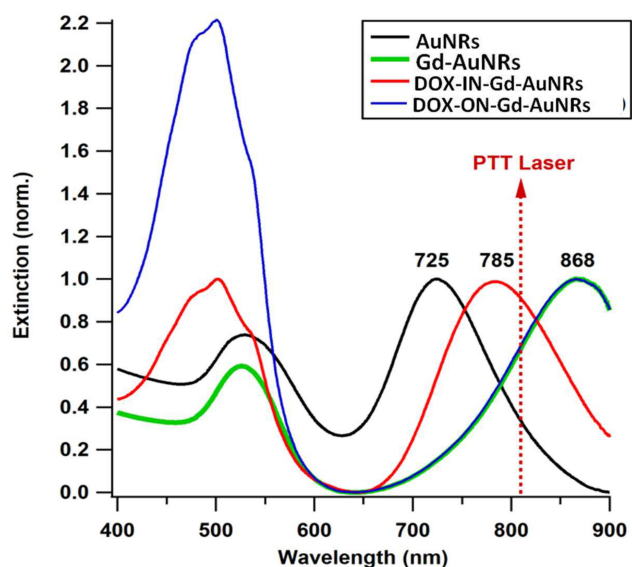


**Figure 5** Normalized UV-Vis extinction spectra of AuNRs, Gd-AuNRs, DOX IN-Gd-AuNRs and DOX ON-Gd-AuNRs.

near-infrared light absorbed by the AuNRs is converted to a thermal energy that leads to a rise of the nanoparticle temperature, hence, the surrounding medium (buffer).

As shown in Figure 6, the temperature of the control solutions (buffer, without AuNRs) is very weak ( $<0.4^{\circ}\text{C}$ ) due to the absence of the thermoplasmonic effect. While

the temperature elevation of the four AuNRs solutions is much higher than the limit of  $4^{\circ}\text{C}$  (minimum temperature required for the photothermal effect).<sup>64</sup> These results also show that, when the LSPR wavelength is close to the incident laser wavelength (808 nm), the optical-thermal energy conversion can be significantly enhanced. The temperature elevation in DOXIN-Gd-AuNRs (IN) solution (LSPR at 780 nm) is higher than AuNRs solution (LSPR at 725 nm). The temperature elevation in the DOX ON-Gd-AuNRs solution (LSPR at 868 nm) is much lower than the temperature with DOX IN-Gd-AuNRs for the same reason.

## Conclusion

In this paper, we have developed a novel theranostic nanoparticle composed of gadolinium complexes to gold ions, with a PEG biopolymer matrix conjugated with antitumoral doxorubicin, providing multifunctional therapeutic features. Exhaustive physicochemical characterization studies were conducted showing a mid size of 20 to 40 nm diameters obtained with low polydispersity, efficient synthesis using seed mediated synthesis with chelation reaction with high scale-up, long duration stability, specific doxorubicin release with acidic pH, strong photothermal abilities at 808 nm in the NIR transparency window, strong magnetic  $r_1$  relaxivities for positive MRI, well adapted for image-guided therapy and

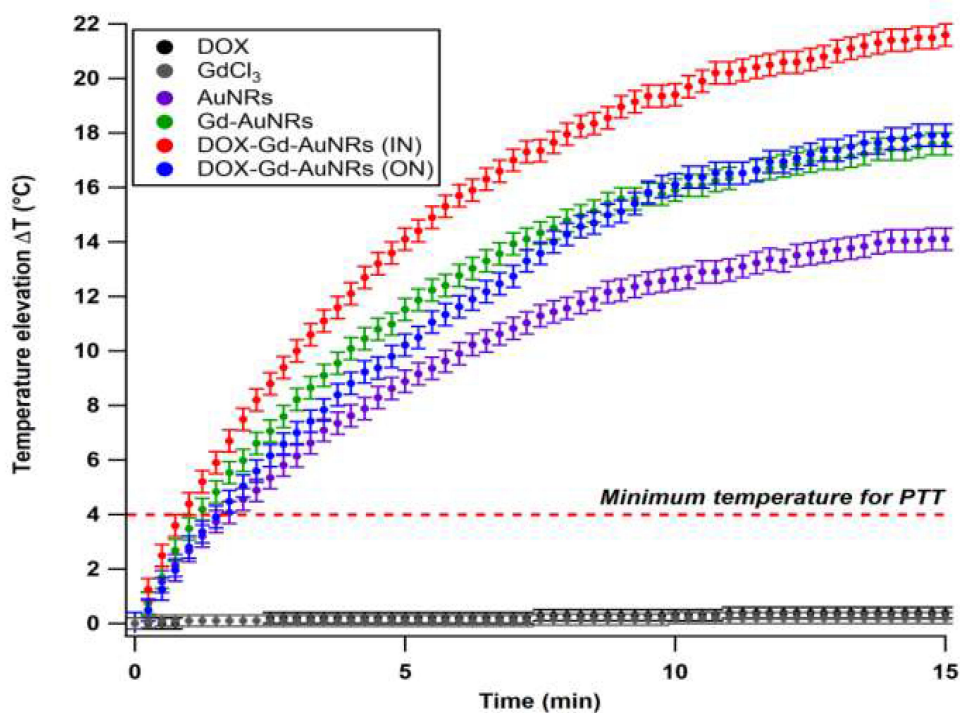


**Figure 6** Time-dependant temperature elevation of AuNRs, Gd-AuNRs, DOX IN Gd-AuNRs, DOXGd-AuNRs and DOX ON Gd-AuNRs, and control solutions (buffers alone: DOX and GdCl<sub>3</sub>) under 808 nm laser ( $0.5 \text{ W cm}^{-2}$ ). The temperature elevation of NRs is higher than the minimum temperature required for PTT ( $+4^{\circ}\text{C}$ ).

therapeutical purpose in biological tissues. Particularly, these nano conjugates enhanced the cytotoxicity toward tumoral MIAPaCa-2 cells by a factor of 320 compared to doxorubicin alone. Moreover, MRI T<sub>1</sub> features at 7T enables interesting positive contrast for bioimaging and their adapted size potential passive targeting to tumors by Enhanced Permeability Retention. Given these encouraging antitumoral and imaging properties, this bimetallic theranostic nanomaterial system represents a veritable promise as a therapeutic entity in the field of medicinal applications.

## Acknowledgment

This research was partially supported by the structure fédérative de recherche NAP MOSAIC of the University Sorbonne Paris Nord. The MRI experiments were performed at the LIOPA/MRI imaging facility of the consortium Plateformes d'Imageries du Vivant of Paris Descartes, PIV and UTCBS/SEISAD/ENSCP team. The IDEX SPC Sorbonne Paris Cité IDV Imageries du Vivant is also acknowledged. We also thank la Ligue Contre le Cancer for financing MK's thesis, and the Ecole Doctorale of Université PSL, U406 for financing SB's thesis.

## Disclosure

The authors report no conflicts of interest in this work.

## References

- Cobley CM, Chen J, Cho EC, Wang LV, Xia Y. Gold nanostructures: a class of multifunctional materials for biomedical applications. *Chem Soc Rev*. 2011;40(1):44–56. doi:10.1039/B821763G
- Cai H, Dai X, Wang X, et al. A nanostrategy for efficient imaging-guided antitumor therapy through a stimuli-responsive branched polymeric prodrug. *Adv Sci*. 2020;7(6):1903243. doi:10.1002/advs.201903243
- Howard TV, Dunklin JR, Forcherio GT, Roper DK. Thermoplasmonic dissipation in gold nanoparticle-polyvinylpyrrolidone thin films. *RSC Adv*. 2017;7(89):56463–56470. doi:10.1039/C7RA03892E
- Zhang X, Wu Y, Li Z, et al. Glycodendron/pyropheophorbide-a (Ppa)-functionalized hyaluronic acid as a nanosystem for tumor photodynamic therapy. *Carbohydr Polym*. 2020;247:116749. doi:10.1016/j.carbpol.2020.116749
- Zhang J, Mou L, Jiang X. Surface chemistry of gold nanoparticles for health-related applications. *Chem Sci*. 2020;11(4):923–936. doi:10.1039/C9SC06497D
- Cai H, Xiang Y, Zeng Y, et al. Cathepsin B-responsive and gadolinium-labeled branched glycopolymers-PTX conjugate-derived nanotheranostics for cancer treatment. *Acta Pharmaceutica Sinica B*. 2020.
- Jabir M, Sahib UI, Taqi Z, et al. Linalool-loaded glutathione-modified gold nanoparticles conjugated with CALNN peptide as apoptosis inducer and NF- $\kappa$ B translocation inhibitor in SKOV-3 cell line. *Int J Nanomedicine*. 2020;15:9025–9047. doi:10.2147/IJN.S276714
- Al-Dulimi AG, Al-Saffar AZ, Sulaiman GM, et al. Immobilization of l-asparaginase on gold nanoparticles for novel drug delivery approach as anti-cancer agent against human breast carcinoma cells. *J Mater Res Technol*. 2020;9(6):15394–15411.
- Sulaiman GM, Waheeb HM, Jabir MS, Khazaal SH, Dewir YH, Naidoo Y. Hesperidin loaded on gold nanoparticles as a drug delivery system for a successful biocompatible, anti-cancer, anti-inflammatory and phagocytosis inducer model. *Sci Rep*. 2020;10(1):9362. doi:10.1038/s41598-020-66419-6
- Yeh Y-C, Creran B, Rotello VM. Gold nanoparticles: preparation, properties, and applications in bionanotechnology. *Nanoscale*. 2012;4(6):1871–1880. doi:10.1039/C1NR11188D
- Zhang X-F, Liu Z-G, Shen W, Gurunathan S. Silver nanoparticles: synthesis, characterization, properties, applications, and therapeutic approaches. *Int J Mol Sci*. 2016;17(9):1534. doi:10.3390/ijms17091534
- Ali A, Zafar H, Zia M, et al. Synthesis, characterization, applications, and challenges of iron oxide nanoparticles. *Nanotechnol Sci Appl*. 2016;9:49–67. doi:10.2147/NSA.S99986
- Hou H, Chen L, He H, Chen L, Zhao Z, Jin Y. Fine-tuning the LSPR response of gold nanorod-polyaniline core-shell nanoparticles with high photothermal efficiency for cancer cell ablation. *J Mater Chem B*. 2015;3(26):5189–5196. doi:10.1039/C5TB00556F
- Thierry B, Ng J, Krieg T, Griesser HJ. A robust procedure for the functionalization of gold nanorods and noble metal nanoparticles. *Chem Commun*. 2009;(13):1724–1726. doi:10.1039/b820137d
- Pan L, Liu J, Shi J. Nuclear-targeting gold nanorods for extremely low NIR activated photothermal therapy. *ACS Appl Mater Interfaces*. 2017;9(19):15952–15961. doi:10.1021/acsami.7b03017
- Kim HS, Lee DY. Near-infrared-responsive cancer photothermal and photodynamic therapy using gold nanoparticles. *Polymers*. 2018;10(9):961. doi:10.3390/polym10090961
- Bi C, Chen J, Chen Y, et al. Realizing a record photothermal conversion efficiency of spiky gold nanoparticles in the second near-infrared window by structure-based rational design. *Chem Mater*. 2018;30(8):2709–2718. doi:10.1021/acs.chemmater.8b00312
- Mackey MA, Ali MRK, Austin LA, Near RD, El-Sayed MA. The most effective gold nanorod size for plasmonic photothermal therapy: theory and in vitro experiments. *J Phys Chem B*. 2014;118(5):1319–1326. doi:10.1021/jp409298f
- Xiao Y, Hong H, Matson VZ, et al. Gold nanorods conjugated with doxorubicin and cRGD for combined anticancer drug delivery and PET imaging. *Theranostics*. 2012;2(8):757–768. doi:10.7150/thno.4756
- Cai F, Luis MAF, Lin X, et al. Anthracycline-induced cardiotoxicity in the chemotherapy treatment of breast cancer: preventive strategies and treatment (Review). *Mol Clin Oncol*. 2019;11(1):15–23. doi:10.3892/mco.2019.1854
- Hwang T, Han HD, Song CK, et al. Anticancer drug-phospholipid conjugate for enhancement of intracellular drug delivery. *Macromol Symp*. 2007;249–250(1):109–115. doi:10.1002/masy.200750318
- Sun H, Guo X, Zeng S, et al. A multifunctional liposomal nanoplat-form co-delivering hydrophobic and hydrophilic doxorubicin for complete eradication of xenografted tumors. *Nanoscale*. 2019;11(38):17759–17772. doi:10.1039/C9NR04669K
- Venkatesan R, Pichaimani A, Hari K, Balasubramanian PK, Kulandaivel J, Premkumar K. Doxorubicin conjugated gold nanorods: a sustained drug delivery carrier for improved anticancer therapy. *J Mater Chem B*. 2013;1(7):1010–1018. doi:10.1039/C2TB00078D
- Moustaoui H, Movia D, Dupont N, et al. Tunable design of gold(III)-doxorubicin complex-PEGylated nanocarrier. The golden doxorubicin for oncological applications. *ACS Appl Mater Interfaces*. 2016;8(31):19946–19957. doi:10.1021/acsami.6b07250
- Monteil M, Moustaoui H, Picardi G, et al. Polyphosphonate ligands: from synthesis to design of hybrid PEGylated nanoparticles toward phototherapy studies. *J Colloid Interface Sci*. 2018;513:205–213. doi:10.1016/j.jcis.2017.10.055
- Morel A-L, Giraud S, Bialecki A, Moustaoui H, de La Chapelle ML, Spadavecchia J. Green extraction of endemic plants to synthesize gold nanoparticles for theranostic applications. *Front Lab Med*. 2017;1(3):158–171. doi:10.1016/j.flm.2017.10.003

27. Spadavecchia J, Movia D, Moore C, et al. Targeted polyethylene glycol gold nanoparticles for the treatment of pancreatic cancer: from synthesis to proof-of-concept in vitro studies. *Int J Nanomedicine*. 2016; 11:791–822. doi:10.2147/IJN.S97476
28. Liu H, Jiang P, Li Z, Li X, Djaker N, Spadavecchia J. HIV-1 tat peptide-gemcitabine gold (III)-PEGylated complex—nanoflowers: a sleek thermosensitive hybrid nanocarrier as prospective anticancer. *Part Part Syst Charact*. 2018;35(8):1800082. doi:10.1002/ppsc.201800082
29. Sahli F, Courcelle M, Palama T, Djaker N, Savarin P, Spadavecchia J. Temozolomide, gemcitabine, and decitabine hybrid nanoconjugates: from design to proof-of-concept (PoC) of synergies toward the understanding of drug impact on human glioblastoma cells. *J Med Chem*. 2020;63(13):7410–7421. doi:10.1021/acs.jmedchem.0c00694
30. Aouidat F, Boumati S, Khan M, Tielens F, Doan B-T, Spadavecchia J. Design and synthesis of gold-gadolinium-core-shell nanoparticles as contrast agent: a smart way to future nanomaterials for nanomedicine applications. *Int J Nanomedicine*. 2019;14:9309–9324. doi:10.2147/IJN.S224805
31. Falk Delgado A, Van Westen D, Nilsson M, et al. Diagnostic value of alternative techniques to gadolinium-based contrast agents in MR neuroimaging—a comprehensive overview. *Insights Imaging*. 2019;10(1):84. doi:10.1186/s13244-019-0771-1
32. Boros E, Gale EM, Caravan P. MR imaging probes: design and applications. *Dalton Transact (Cambridge, England: 2003)*. 2015;44(11):4804–4818. doi:10.1039/C4DT02958E
33. Jacques V, Dumas S, Sun W-C, Troughton JS, Greenfield MT, Caravan P. High-relaxivity magnetic resonance imaging contrast agents. Part 2. Optimization of inner- and second-sphere relaxivity. *Invest Radiol*. 2010;45(10):613–624. doi:10.1097/RLL.0b013e3181ee6a49
34. Bouron A, Kiselyov K, Oberwinkler J. Permeation, regulation and control of expression of TRP channels by trace metal ions. *Pflugers Arch*. 2015;467(6):1143–1164.
35. Wahsner J, Gale EM, Rodríguez-Rodríguez A, Caravan P. Chemistry of MRI contrast agents: current challenges and new frontiers. *Chem Rev*. 2019;119(2):957–1057. doi:10.1021/acs.chemrev.8b00363
36. Tweedle MF. The chemistry of contrast agents in medical magnetic resonance imaging edited by André E. Merbach and Éva Tóth (University of Lausanne). J. Wiley & Sons: chichester, New York, Weinheim, Brisbane, Singapore, Toronto. 2001. xii + 472 pp. \$160.00. ISBN: 0-471-60778-9. *J Am Chem Soc*. 2002;124(5):884–885.
37. Edogun O, Nguyen NH, Halim M. Fluorescent single-stranded DNA-based assay for detecting unchelated Gadolinium(III) ions in aqueous solution. *Anal Bioanal Chem*. 2016;408(15):4121–4131. doi:10.1007/s00216-016-9503-2
38. Yang C-T, Padmanabhan P, Gulyás BZ. Gadolinium(iii) based nanoparticles for T1-weighted magnetic resonance imaging probes. *RSC Adv*. 2016;6(65):60945–60966. doi:10.1039/C6RA07782J
39. Song Y, Xu X, MacRenaris KW, Zhang X-Q, Mirkin CA, Meade TJ. Multimodal gadolinium-enriched DNA–gold nanoparticle conjugates for cellular imaging. *Angewandte Chemie Int Edition*. 2009;48(48):9143–9147. doi:10.1002/anie.200904666
40. Liu Y, Tang Y, Tian Y, et al. Gadolinium-doped hydroxyapatite nanorods as T1 contrast agents and drug carriers for breast cancer therapy. *ACS Appl Nano Mater*. 2019;2(3):1194–1201. doi:10.1021/acsanm.8b02036
41. Spadavecchia J, Apchain E, Alberic M, Fontan E, Reiche I. One-step synthesis of collagen hybrid gold nanoparticles and formation on Egyptian-like gold-plated archaeological ivory. *Angew Chem Int Ed Engl*. 2014;53(32):8363–8366. doi:10.1002/anie.201403567
42. Haddada MB, Movia D, Prina-Mello A, Spadavecchia J. Docetaxel gold complex nanoflowers: a chemo-biological evaluation for their use as nanotherapeutics. *Colloids Surf B Biointerfaces*. 2020;194(111172):111172. doi:10.1016/j.colsurfb.2020.111172
43. Vigderman L, Zubarev ER. High-yield synthesis of gold nanorods with longitudinal SPR peak greater than 1200 nm using hydroquinone as a reducing agent. *Chem Mater*. 2013;25(8):1450–1457. doi:10.1021/cm303661d
44. Wang Y, Long S, Vdović S, Wang X. Fine tuning of the longitudinal plasmon resonance of gold nanorods by depleting gold precursor. *Chem Mater*. 2013;25(8):1372–1376. doi:10.1021/cm301832d
45. Villar-Alvarez E, Cambón A, Pardo A, et al. Gold nanorod-based nanohybrids for combinatorial therapeutics. *ACS Omega*. 2018;3(10):12633–12647. doi:10.1021/acsomega.8b01591
46. Melani V, Haddada MB, Moustouli H, et al. Pegylated doxorubicin gold complex: from nanovector to potential intercalant agent for biosensor applications. *Front Lab Med*. 2017;1(3):114–121. doi:10.1016/j.flm.2017.06.004
47. Spadavecchia J, Casale S, Boujday S, Pradier C-M. Bioconjugated gold nanorods to enhance the sensitivity of FT-SPR-based biosensors. *Colloids Surf B Biointerfaces*. 2012;100:1–8. doi:10.1016/j.colsurfb.2012.03.035
48. Li H, Su Y, Li L, Strachan DM. Raman spectroscopic study of gadolinium(III) in sodium-aluminoborosilicate glasses. *J Non Cryst Solids*. 2001;292(1):167–176. doi:10.1016/S0022-3093(01)00878-X
49. Kumar S, Meena VK, Hazari PP, Sharma RK. PEG coated and doxorubicin loaded multimodal Gadolinium oxide nanoparticles for simultaneous drug delivery and imaging applications. *Int J Pharm*. 2017;527(1–2):142–150. doi:10.1016/j.ijpharm.2017.05.027
50. Amreddy N, Muralidharan R, Babu A, et al. Tumor-targeted and pH-controlled delivery of doxorubicin using gold nanorods for lung cancer therapy. *Int J Nanomedicine*. 2015;10:6773–6788. doi:10.2147/IJN.S93237
51. Malikova H. Nephrogenic systemic fibrosis: the end of the story? *Quant Imaging Med Surg*. 2019;9(8):1470–1474. doi:10.21037/qims.2019.07.11
52. Barge A, Cravotto G, Gianolio E, Fedeli F. How to determine free Gd and free ligand in solution of Gd chelates. A technical note. *Contrast Media Mol Imaging*. 2006;1(5):184–188. doi:10.1002/cmim.110
53. Zhang R-C, Sun D, Zhang R, et al. Gold nanoparticle-polymer nanocomposites synthesized by room temperature atmospheric pressure plasma and their potential for fuel cell electrocatalytic application. *Sci Rep*. 2017;7(1):46682. doi:10.1038/srep46682
54. Khadir S, Diallo A, Chakaroun M, Boudrioua A. Exciton enhancement and exciplex quenching by plasmonic effect of Aluminum nanoparticle arrays in a blue organic light emitting diode. *Opt Express*. 2017;25(9):9812–9822. doi:10.1364/OE.25.009812
55. Barnes WL, Dereux A, Ebbesen TW. Surface plasmon subwavelength optics. *Nature*. 2003;424(6950):824–830. doi:10.1038/nature01937
56. Baffou G, Quidant R. Thermo-plasmonics: using metallic nanostructures as nano-sources of heat. *Laser Photon Rev*. 2013;7(2):171–187. doi:10.1002/lpor.201200003
57. Baffou G, Quidant R, García de Abajo FJ. Nanoscale control of optical heating in complex plasmonic systems. *ACS Nano*. 2010;4(2):709–716. doi:10.1021/nn901144d
58. Link S, El-Sayed MA. Spectral properties and relaxation dynamics of surface plasmon electronic oscillations in gold and silver nanodots and nanorods. *J Phys Chem B*. 1999;103(40):8410–8426. doi:10.1021/jp9917648
59. Sheng Y, Lin M, Li X, et al. Enhancement of the 808 nm photothermal effect of gold nanorods by thiol-induced self-assembly. *Part Part Syst Charact*. 2014;31(7):788–793. doi:10.1002/ppsc.201300351
60. Yang S, Palanikumar L, Jeong S, et al. Synergistic effect of photothermal therapy and chemotherapy using camptothecin-conjugated gold nanorods. *Part Part Syst Charact*. 2018;35(2):1700307. doi:10.1002/ppsc.201700307
61. Djaker N, Sultana S, Issaad D, et al. Spherical and flower-shaped gold nanoparticles characterization by scattering correlation spectroscopy. *J Phys Chem C*. 2016;120(21):11700–11708. doi:10.1021/acs.jpcc.6b02436

62. Issaad D, Moustauoui H, Medjahed A, et al. Scattering correlation spectroscopy and raman spectroscopy of thiophenol on gold nanoparticles: comparative study between nanospheres and nanourchins. *J Phys Chem C*. 2017;121(33):18254–18262. doi:10.1021/acs.jpcc.7b05355
63. Moustauoui H, Saber J, Djeddi I, et al. In situ protein corona study by scattering correlation spectroscopy: a comparative study between spherical and urchin-shaped gold nanoparticles. *Nanoscale*. 2019;11:3665–3673. doi:10.1039/C8NR09891C
64. Jaque D, Martinez Maestro L, Del Rosal B, et al. Nanoparticles for photothermal therapies. *Nanoscale*. 2014;6(16):9494–9530.

### International Journal of Nanomedicine

Dovepress

### Publish your work in this journal

The International Journal of Nanomedicine is an international, peer-reviewed journal focusing on the application of nanotechnology in diagnostics, therapeutics, and drug delivery systems throughout the biomedical field. This journal is indexed on PubMed Central, MedLine, CAS, SciSearch®, Current Contents®/Clinical Medicine,

Journal Citation Reports/Science Edition, EMBase, Scopus and the Elsevier Bibliographic databases. The manuscript management system is completely online and includes a very quick and fair peer-review system, which is all easy to use. Visit <http://www.dovepress.com/testimonials.php> to read real quotes from published authors.

Submit your manuscript here: <https://www.dovepress.com/international-journal-of-nanomedicine-journal>